JOURNAL OF SPACECRAFT AND ROCKETS
Vol. 32, No. 5, September–October 1995

Simulation and Shuttle Hitchhiker Validation of Passive Satellite Aerostabilization

Renjith R. Kumar,* Daniel D. Mazanek,† and Michael L. Heck*
Analytical Mechanics Associates, Inc., Hampton, Virginia 23666

The Passive Aerodynamically Stabilized Magnetically Damped Satellite experiment will characterize and demonstrate passive aerodynamic stabilization and passive magnetic hysteresis damping of attitude rates. It is currently scheduled to be deployed on a Shuttle Hitchhiker flight. Although theoretically feasible, aerodynamically induced passive attitude stability represents a technology that has never been substantiated through actual flight experience. The two-week experiment will serve to validate overall performance predictions by the high-fidelity free-molecular-flow simulation code developed at the Langley Research Center of NASA. The code can simulate with high fidelity the flight characteristics of a satellite in low Earth orbit. Aerostabilization, if proved, is highly desirable for future missions such as the Gravity and Magnetic Earth Surveyor. This paper describes the simulator, simulation results, and the Hitchhiker experiment in the context of the Gravity and Magnetic Earth Surveyor subsatellite aerostabilization requirements.

Nomenclature

a = equatorial radius of Earth
B = induced flux density on permeable rod
B_m = saturation flux density of permeable rod
B_0 = remanance of permeable rod
dA_i = area of ith surface element
$d\boldsymbol{F}_i$ = aerodynamic force vector on the ith surface element
dm = elemental mass of incoming air molecules
$d\boldsymbol{S}_i$ = solar force vector on the ith surface element
$d\boldsymbol{T}_{Ai}$ = aerodynamic torque vector on the ith surface element
$d\boldsymbol{T}_{Si}$ = solar torque vector on the ith surface element
dt = differential time element
g_n^m, h_n^m = empirically determined Gaussian coefficients
H = scalar magnetizing field along longitudinal axis of permeable rod
$\boldsymbol{H}$ = Earth's magnetic field vector at satellite location
H_0 = coercive force of permeable rod
$\boldsymbol{M}$ = vector dipole moment induced on all rods
$\hat{\boldsymbol{n}}_i$ = inward surface normal unit vector of ith surface element
P_n^m = Legendre functions (Schmidt-normalized)
p = solar pressure constant
Q = scalar potential function of Earth's magnetic field
r = geocentric distance to satellite
$\boldsymbol{r}_i$ = position vector of center of area of ith surface element with respect to center of mass of satellite
$\hat{\boldsymbol{S}}$ = unit vector along sun–satellite line of sight
$\boldsymbol{T}_D$ = magnetic damping torque vector
$\hat{\boldsymbol{t}}_i$ = tangential unit vector of ith surface element
V = magnitude of velocity of incoming air molecules
$\boldsymbol{V}$ = velocity vector of incoming air molecules
$\hat{\boldsymbol{V}}$ = unit velocity vector of incoming air molecules
V_B = mean velocity magnitude of diffusely reflected air molecules
$\boldsymbol{V}_f^D$ = velocity vector of diffused reflected components of air molecules
$\boldsymbol{V}_f^S$ = velocity vector of specularly reflected components of air molecules
α_i = angle between $\boldsymbol{V}$ and $\hat{\boldsymbol{n}}_i$
β = cone angle of the satellite
θ = coelevation of satellite
ϱ = density of air
σ = ratio of photons reflected diffusively to total photons reflected
σ_A = ratio of photons absorbed to incoming photons
σ_B = ratio of V_B to V
σ_D = ratio of number of accommodated air molecules to incoming air molecules
ϕ = east longitude from Greenwich of satellite

Received Nov. 14, 1994; revision received March 15, 1995; accepted for pulication March 15, 1995.

*Senior Engineer. Member AIAA.
†Senior Project Engineer.

Background

CURRENTLY the trend is away from large, multipayload platforms to small single- or dual-instrument microsatellites. Passive attitude stability and control are highly desirable from a cost, weight, power, and reliability point of view when contrasted with active attitude control systems. For the class of missions that require a local vertical, Earth-oriented attitude, two approaches have been suggested for providing all-passive attitude stability: gravity-gradient and aerodynamic (or some combination thereof). Gravity-gradient configurations tend to have large mass and boom requirements, higher orbit decay rates, weak yaw-channel stiffness, and poor pitch-channel stability characteristics in the presence of magnetic hysteresis damping. Although not yet flight-demonstrated, premission analysis indicates that aerostabilization can provide pitch and yaw attitude stability to within a few degrees, depending on altitude and orbital-inclination-dependent rotating atmosphere effects. While providing an attitude restoring torque much like that on a wind vane in a sufficiently dense atmosphere, aerodynamically induced forces and torques are not capable of dissipating energy; hence, attitude rate damping devices such as magnetic hysteresis rods are required to remove any initial tipoff rates or off-nominal attitude dispersions that may occur during deployment or result from external perturbations.

Relevance

An immediate application of a passive aerodynamically stabilized magnetically damped subsatellite is the Gravity and Magnetic Earth Surveyor[1] (GAMES) mission. This concept was envisioned as a low-cost, low-weight, long-lifetime option for the subsatellite that is completely passive and carries a corner-cube retroreflector[2] on its front face. The retroreflector reflects the laser beam projected on it by an active main satellite. The range rate between the two satellites is used to evaluate the gravity field to very fine precision. The main satellite performs stationkeeping with respect to the subsatellite at a distance of 200 km (±50 km) in a circular orbit of altitude varying from 325 to 250 km because of drag decay. The relative positions of the satellites in the GAMES mission scenario are shown in Fig. 1.

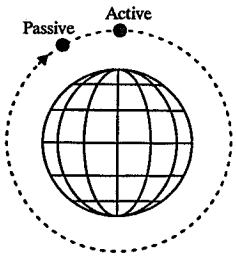

Fig. 1 GAMES mission scenario.

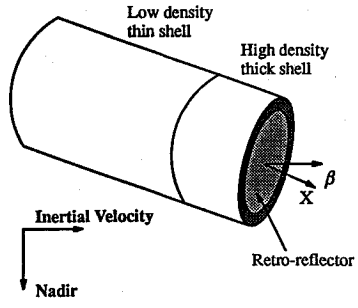

Fig. 2 GAMES–PAMS subsatellite schematic.

The orbit inclination chosen is 87 deg in order to span most of the globe.

A mission requirement imposed on the subsatellite attitude performance is that the cone angle, defined as the angle between the inertial velocity vector and the subsatellite body X axis, as shown in Fig. 2, be "small." No restriction is imposed on the roll angle of the spacecraft. The mass distribution properties of the subsatellite are such that all three inertias are equal, resulting in no gravity-gradient torque, and most of the mass is forward of the geometric center of the satellite, resulting in a center-of-pressure–center-of-mass offset that provides sufficient pitch and yaw aero restoring torques.

Since aerostabilization and hysteresis damping through miniature hysteresis rods is desirable for the GAMES mission and since the mission is fairly expensive, the proof of concept of aerostabilization and hysteresis damping need to be demonstrated by preflight simulations and experiments. The preflight simulations are performed using a high-fidelity simulator (FREEMOL) developed by the authors. The Passive Aerodynamically Stabilized Magnetically Damped Satellite (PAMS) Hitchhiker experiment would be the first flight experiment to demonstrate the concept of passive aerostabilization. This paper begins with a description of the high-fidelity simulator, followed by some simulation results for the GAMES nominal subsatellite and the current PAMS design. The PAMS Hitchhiker experiment and its purpose for corroborating the "concept" and the simulator are also discussed.

High-Fidelity Simulator

The high-fidelity simulator models the following phenomena to simulate the attitude dynamics of the sub-satellite:

1) Free-molecular-flow aerodynamics: accommodation; specular and diffuse reflection of air molecules with shadowing.

2) Jacchia atmospheric model: varying flux and geomagnetic index.

3) Horizontal global winds.

4) Solar radiation pressure: absorption; specular and diffuse reflection of photons with shadowing.

5) Eight-order Earth magnetic field.

6) Magnetic hysteresis rods.

7) Orbital dynamics: altitude decay, regression of ascending node, and changing solar geometry.

Aerodynamic Model

For altitudes varying from 325 to 250 km, the mean free path of the air molecules is on the order of 1 km. Thus the molecules impinging on the surface of the satellite and the molecules outgoing from the surface can be dealt with separately. Free-molecular-flow aerodynamics[3] is used to model the aerodynamic drag and torque acting on the satellite under these circumstances. This model relies on the kinetic theory of gases, and it is at the far end of the rarefaction spectrum from the more conventional continuum-flow model.

Air molecules transfer momentum to the surface either by specular reflection or by diffuse reflection. The former is a deterministic process where each molecule bounces off the surface with no change in energy. The angle of reflection equals the angle of incidence. Moreover, the incoming velocity vector, the outgoing velocity vector, and the surface normal are coplanar. Only few of the molecules experience specular reflection. More often, diffuse reflection occurs, where the incoming molecules, which are partially accommodated to the surface, lose memory of the incoming direction and energy and mingle with the other molecules in the surface. The molecules then depart with a probabilistic energy dependent upon the surface temperature and a probabilistic direction governed by the cosine rule.

The momentum-transfer equation on the ith surface element of the satellite that is not shadowed with respect to the wind vector may be written as

$$\mathrm{d}m\,\boldsymbol{V} - \int \mathrm{d}\boldsymbol{F}_i\,\mathrm{d}t = \sigma_D\,\mathrm{d}m\,\boldsymbol{V}_f^D + (1-\sigma_D)\,\mathrm{d}m\,\boldsymbol{V}_f^S \tag{1}$$

which can be rearranged to provide the force acting on the ith element as

$$\mathrm{d}\boldsymbol{F}_i = \frac{\mathrm{d}m}{\mathrm{d}t}\left[\boldsymbol{V} - \sigma_D\boldsymbol{V}_f^D - (1-\sigma_D)\boldsymbol{V}_f^S\right] \tag{2}$$

Here $\sigma_D = 1.0$ corresponds to total accommodation, and $\sigma_D = 0.0$ simulates total specular reflection. Aerothermodynamicists believe[3] that the best estimate of σ_D for the altitudes of interest (250–450 km) is between 0.8 and 0.9. To be conservative, the authors assume a feasible range of 0.6 to 1.0. The mass flow rate can be written as

$$\frac{\mathrm{d}m}{\mathrm{d}t} = \varrho V\cos\alpha_i\,\mathrm{d}A_i \tag{3}$$

The tangential unit vector is normal to $\hat{\boldsymbol{n}}_i$ and is coplanar with $\boldsymbol{V}$ and $\hat{\boldsymbol{n}}_i$. Explicitly,

$$\sin\alpha_i\,\hat{\boldsymbol{t}}_i = \hat{\boldsymbol{V}} - \cos\alpha_i\,\hat{\boldsymbol{n}}_i \tag{4}$$

The incoming velocity vector can be written as

$$\boldsymbol{V} = V(\cos\alpha_i\,\hat{\boldsymbol{n}}_i + \sin\alpha_i\,\hat{\boldsymbol{t}}_i) \tag{5}$$

The partially accommodated molecules leaving the surface via diffuse reflection have no mean motion in the $\hat{\boldsymbol{t}}_i$ direction, but have a mean velocity in the $-\hat{\boldsymbol{n}}_i$ direction given by

$$\boldsymbol{V}_f^D = -V_B\hat{\boldsymbol{n}}_i \tag{6}$$

which is characteristic of the surface temperature. The coefficient σ_B is defined by

$$\sigma_B = (V_B/V) \tag{7}$$

Here $\sigma_B = 0.0$ implies that the re-emitted molecules bleed off with zero momentum. In practice σ_B is estimated to range from 0.0 to 0.1, with a nominal value[3] of 0.05.

The velocity of the specularly reflected molecules is given by

$$\boldsymbol{V}_f^S = V(-\cos\alpha_i\,\hat{\boldsymbol{n}}_i + \sin\alpha_i\,\hat{\boldsymbol{t}}_i) \tag{8}$$

The aerodynamic torque on the satellite due to the force on the ith element is given by the cross product

$$\mathrm{d}\boldsymbol{T}_{Ai} = \boldsymbol{r}_i \times \mathrm{d}\boldsymbol{F}_i \tag{9}$$

The satellite is initially designed using computer-aided-design (CAD) tools, and the surface is discretized into a mesh consisting of small triangles as shown in Fig. 3. Prior to simulation, for different cone and clock angles of the relative wind vector with respect to the body, shadowing information on each mesh element is evaluated

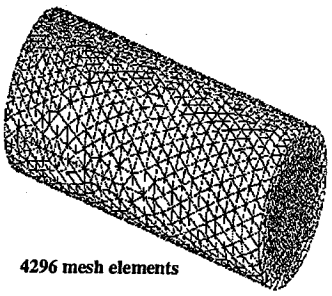

Fig. 3 Meshed GAMES subsatellite.

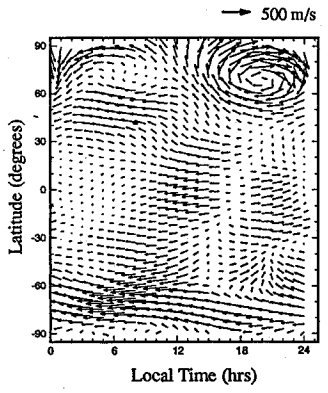

Fig. 4 Sample global wind pattern.

via a ray-tracing algorithm. For each discretized cone and clock angle, the normalized aerodynamic forces and torques are evaluated on each element and then summed. At any instant of time during the simulation, the relative wind vector with respect to the body is evaluated, and the normalized aerodynamic forces and torques corresponding to the particular cone and clock angle are interpolated from splined data. The actual aerodynamic forces and torques are then obtained by multiplying the normalized values by the dynamic pressure.

As a historical note, during the final phase of the Skylab mission, careful modeling of the aerodynamic forces and torques and the gravity-gradient torques acting on Skylab was performed[4–6] in order to predict the lifetime and the nature of attitude oscillations for a possible 1979 Space Shuttle visit to salvage the satellite from altitude decay. The aerodynamic moment coefficients were evaluated from a Fourier series curve fit[7] of observed data, the luxury of which is lacking for the proposed GAMES and PAMS mission.

Since aerodynamic forces and torques acting on the satellite significantly affect attitude stability characteristics, a solar-activity-dependent Jacchia atmospheric density model[8] is employed. This code accepts predicted solar flux and geomagnetic index data.[9] The atmospheric diurnal bulge is modeled, which is characterized by maximum daytime density at about 2 p.m. local solar time, at a latitude dependent on the time of year. Based on the orbital inclination and ascending node, variations in atmospheric density of several hundred percent over a 90-min orbit can arise from the diurnal bulge effect. Variations in atmospheric density due to the interaction of the solar wind with the Earth's magnetic field as a function of the geomagnetic activity are also modeled. These density variations are of critical significance to resonant restoring-torque behavior.

The effect of global horizontal winds must also be allowed for when determining the aerodynamic flight characteristics of the passively stabilized satellite. Like the Jacchia atmospheric density model, the global horizontal wind model[10] accepts solar flux and geomagnetic index as input to compute mean horizontal wind magnitudes and directions as a function of latitude and local time. Especially significant for missions having high orbital inclinations, polar storms of up to 600-m/s velocity can be simulated in this manner. Figure 4 depicts a sample horizontal windstorm at an altitude of 250 km.

Solar-Pressure Model

It is also important to correctly model the effects of solar radiation pressure on the satellite. Although the net force on the satellite is generally smaller than that due to aerodynamics at these altitudes, the net torque can be comparable on account of a larger center-of-pressure–center-of-mass offset seen along the satellite–sun line.

The photons emitted by the sun possesses a momentum flux, which is transferred to the surface upon incidence.[3] Some of the radiation is completely absorbed. The coefficient σ_A is used to model the percentage of photons that are absorbed by the satellite. This absorption produces a net force in the sun–satellite direction. Typical Earth orbiting satellites have values that range from 0.0 (total reflection) to 0.4 (partial absorption). Since the satellite surface materials are normally opaque, transmission is not included in deriving the solar radiation forces and torques. Of the fraction $1 - \sigma_A$ that is not absorbed, we assume a fraction σ is reflected diffusively. Depending on the surface material and finish, σ may vary from 0.0 to 1.0. The diffuse reflection produces a net force along the inward normal direction of the surface. The remaining radiation is specularly reflected. The force acting on an unshadowed elemental area due to solar radiation pressure is given by

$$\mathrm{d}\boldsymbol{S}_i = p\,\mathrm{d}A_i \cos\alpha_i \left[(\sigma_a + \sigma_{rD})\hat{\boldsymbol{S}} + \left(\tfrac{2}{3}\sigma_{rD} + 2\sigma_{rS}\cos\alpha_i\right)\hat{\boldsymbol{n}}_i\right] \quad (10)$$

where

$$\sigma_{rD} = \sigma(1 - \sigma_a) \quad (11)$$

$$\sigma_{rS} = (1 - \sigma)(1 - \sigma_a) \quad (12)$$

The solar torque on the satellite due to the solar force on the ith element is given by the cross product

$$\mathrm{d}\boldsymbol{T}_{Si} = \boldsymbol{r}_i \times \mathrm{d}\boldsymbol{S}_i \quad (13)$$

The umbra region resulting from Earth occultation is modeled to simulate the nearly step change in solar-radiation-induced torques that act upon the orbiting satellite.

As in the aerodynamic modeling, the meshed satellite is subject to a ray-tracing algorithm to evaluate shadowing for discretized cone and clock angle of the satellite with respect to the sun–satellite line of sight. At any instant of time during the simulation, if the satellite is not in Earth occultation, the sun vector with respect to the body is evaluated and the solar radiation forces and torques corresponding to the particular cone and clock angle are interpolated from splined data.

Earth Magnetic Model

The mechanism utilized for passive attitude rate damping employs magnetic hysteresis rods.[11] An eighth-order Earth magnetic field[12] was used to simulate the interaction of the hysteresis rods with the geomagnetic field as a function of satellite position, attitude, and angular velocity. The predominant portion of the Earth's magnetic field $\boldsymbol{H}$ can be represented as a gradient of a scalar potential function Q, i.e.,

$$\boldsymbol{H} = -\nabla Q \quad (14)$$

The potential function can be expressed by a series of spherical harmonics,

$$Q(r, \theta, \phi) = a \sum_{n=1}^{n=k} \left(\frac{a}{r}\right)^{n+1} W \quad (15)$$

where

$$W = \sum_{m=0}^{m=n} \left(g_n^m \cos m\phi + h_n^m \sin m\phi\right) P_n^m(\theta) \quad (16)$$

The integers n and m are the degree and order of the magnetic field. Once the Earth's magnetic field is obtained in the local vertical local horizontal (LVLH) coordinate frame, the field in body coordinates is evaluated by a simple transformation.

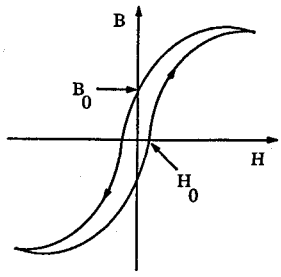

Fig. 5 Schematic of a hysteresis loop.

Model of Magnetic Hysteresis Damping

Magnetic hysteresis rods have been employed successfully in many missions, such as TRANSIT 1B and 2A, for damping attitude rates of orbiting satellites. Since heat is generated as a result of internal friction due to the motion of magnetic domains within permeable materials, a permeable rod spinning in the Earth's magnetic field will experience a hysteresis-induced loss of energy. A schematic of a hysteresis loop is shown in Fig 5. The shape and area of the hysteresis loop depend upon the material used in the rod and on the length-to-diameter ratio of the rod. For example, AEM 4750 offers the greatest energy-dissipating ability[11] of any of the materials tested so far.

The hysteresis model detailed below is based on an induced-flux-density model[13] developed at NASA, GSFC. The saturation flux density denotes the maximum value B can achieve for any value of H. The units for the magnetizing field and the induced flux density are oersteds and gauss, respectively. Given the parameters B_0, H_0, and B_m, the major loop can be defined by

$$B = (2B_m/\pi)\,\tan^{-1}[k(H \pm H_0)] \tag{17}$$

where the + sign corresponds to the left and the − sign to the right boundaries of the major loop; k denotes a dimensionless shaping factor given by

$$k = \tan((\pi B_0/2B_m)/H_0) \tag{18}$$

The slope of the left and right boundaries of the major loop is given by

$$\left(\frac{dB}{dH}\right)_{ml} = \frac{2B_m k}{\pi}\cos^2\left(\frac{\pi B}{2B_m}\right) \tag{19}$$

where the subscript ml refers to the major loop. Now, given a value of B, one can find values for H on the boundaries by solving Eq. (17). These left and right boundary values H_L and H_R are given by

$$H_L = \hat{H} - H_0 \tag{20}$$

$$H_R = \hat{H} + H_0 \tag{21}$$

where

$$\hat{H} = \tan(\pi B/2B_m)/k \tag{22}$$

Now, consider a point inside the major loop boundaries. The slope of the B–H curve passing through that point is given by the following empirical relations:

1) For increasing H, i.e., $dH/dt > 0$,

$$\frac{dB}{dH} = \left(\frac{dB}{dH}\right)_{ml}\left(\frac{H - H_L}{2H_0}\right)^2 \tag{23}$$

2) For decreasing H, i.e., $dH/dt < 0$,

$$\frac{dB}{dH} = \left(\frac{dB}{dH}\right)_{ml}\left(\frac{H_R - H}{2H_0}\right)^2 \tag{24}$$

3) For all cases, then

$$\frac{dB}{dt} = \frac{dB}{dH}\cdot\frac{dH}{dt} \tag{25}$$

Since dH/dt can be evaluated along any direction, Eq. (25) can be used to propagate the induced flux density along the longitudinal axis of any rod. The initial value of B is assumed to lie on the major loop. The above induced flux density is then multiplied by $\text{Vol}/(4\pi \times 10)$, where Vol is the volume of the rod in cubic meters, to obtain the dipole moment. If $\boldsymbol{M}$ denotes the vector dipole moment induced on all rods (usually three orthogonal rods along body axes), then the magnetic damping torque in newton-meters is given by the cross product

$$\boldsymbol{T}_D = \boldsymbol{M} \times \boldsymbol{H} \tag{26}$$

For simulations performed on the GAMES subsatellite and PAMS, a scaled version of the TRANSIT 1B rods is used. The volume is scaled down, assuming the length-to-diameter aspect ratio is maintained. The values of the parameters B_0, H_0, and B_m for the TRANSIT 1B rods[11] are 120, 0.035 Oe, and 2500 G, respectively. A value of B_m equal to 2500 G provides[13] a maximum flux density of 950 G for H varying between ±0.35 Oe.

Orbital Dynamics

The altitude decay is modeled by a simple planar point-mass model. The only forces acting on the satellite are aerodynamic and solar. The regression rate of the ascending node is modeled by a simple analytical function of inclination, altitude, and the Earth oblateness coefficient J_2, assuming a circular orbit. Finally, the sun–Earth geometry is modeled as a function of the day of the year.

Games Simulation Results

The nominal GAMES subsatellite has a mass distribution such that all three moments of inertia are equal, with a center-of-pressure–center-of-mass offset equal to ≈28% of the body length. The center of mass of the satellite is constrained to lie on the vertex of the corner cube to prevent any velocity contribution to the laser-ranging data due to rotational rates of the subsat.

Figure 6 depicts the side view of the GAMES subsat. Following are the original design values of the seven parameters obtained from GSFC:

$$r_i = 3.0 \text{ cm}$$

$$t_f = 1.32 \text{ cm}, \qquad l_f = 8.13 \text{ cm}$$

$$t_b = 0.787 \text{ mm}, \qquad l_b = 11.68 \text{ cm}$$

$$\varrho_f = 18827 \text{ kg/m}^3 \quad \text{(depleted uranium)}$$

$$\varrho_b = 2710 \text{ kg/m}^3 \quad \text{(aluminum)}$$

The center-of-pressure–center-of-mass offset resulting from this nominal design is 5.66 cm. The mass and inertia of the subsat are 4.756 kg and 0.006653 kg · m^2, respectively.

Magnetic hysteresis rod strengths were chosen (three orthogonal rods along each of the body axes—1/6000 the volume of the TRANSIT 1B rod) such that an acceptable damping time of less than 1 week was obtained for worst-case deployment rate errors anticipated, i.e., 0.5 deg/s per axis. Higher strength of hysteresis rods provides quicker damping, but introduces larger steady-state pointing errors, since hysteresis torques are perturbative torques once steady state is achieved. Figure 7 depicts the cone angle of a "nominal" GAMES simulation. The initial orbit is a 325-km circular

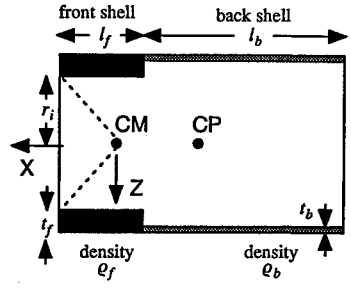

Fig. 6 Nominal GAMES subsatellite.

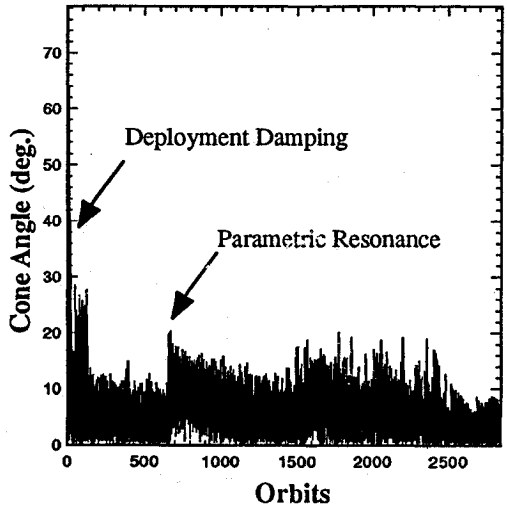

Fig. 7 Nominal GAMES simulation result.

orbit at an inclination of 87 deg and an arbitrary ascending node of −45 deg. Simulation is stopped at an altitude of 250 km. The initial attitude was assumed to be LVLH, but the initial attitude rate errors were 0.5 deg/s per axis. Nominal simulation implies statistical mean values of flux and geomagnetic index for the nominal mission timing with launch on April 1, 1998. The nominal values of the accommodation coefficients are midpoints of the possible range of the coefficients. Statistical mean global winds are also simulated.

Figure 7 indicates that damping is achieved in less than a week, and the subsatellite attitude is stable in pitch and yaw. The cone-angle oscillations are less than 12 deg (95% of the time). The mission lifetime is approximately 6 months. The roll angle locks on to ±45 deg (or ±135 deg in view of symmetry of the y–z rods), and oscillates by ±15 deg. Transients are observed in the cone angle as the subsatellite decays through the altitude. The reason for this behavior is parametric resonance and is explained[14] via a wind-vane analogy and the stability properties of the associated Mathieu–Hill equations.[15]

Lower and upper bounds of aerodynamic and solar accommodation coefficients, as well as $\pm 2\sigma$ atmospheric density conditions, were simulated to study the sensitivity of the cone-angle performance and lifetime to these parameters (all but one parameter held nominal and one parameter shifted to either bound). The 95% cone-angle number varied by ±2 deg, and the lifetime varied from 142 to 236 days (the nominal desirable lifetime being 180 days). The worst-on-worst-case parameters, inferred from this study, provided a 95% cone angle of 13.7 deg and a lifetime of 125 days. This low lifetime is due to the $+2\sigma$ atmosphere, which increases the density and hence the aerodynamic drag.

The attitude dynamics in the presence of external perturbations such as aerodynamic, solar, and magnetic torques are highly nonlinear. Small changes in initial conditions and parameters can make the cone-angle time history change considerably, but the general profile and stability characteristics remain similar. Although the results from the simulator indicate the feasibility of aerodynamic stabilization, it is highly desirable that an experiment be flown to substantiate the claim and to verify if the actual flight data fall within an envelope predicted by the simulator, in regard to the cone angle and deployment damping time.

Shuttle Hitchhiker Validation

The motivation for the PAMS Shuttle experiment is as follows: An entirely passive aerodynamically stabilized satellite has never been flown, and thus represents a technology risk. The analysis methods developed to simulate the free-molecular-flow aerodynamics anticipated over the mission flight regime have not been substantiated by actual flight experience. Furthermore, the utility of miniature magnetic hysteresis rods as rate damping devices has not been established.

The objectives of the Shuttle Hitchhiker experiment are to

1) Characterize the attitude of PAMS in both its initial deployment and steady states.

2) Determine if the above characteristics are within the envelope predicted by the high-fidelity simulator.

3) Evaluate satellite aerodynamic stability and magnetic damping performance for the GAMES mission.

PAMS is ejected out of a Shuttle Hitchhiker GAS (Get Away Special) canister assembly in an unstable attitude mode (−90-deg pitch attitude with respect to local horizontal). The Shuttle payload video system is used to track the general behavior of PAMS during initial deployment. The video system and the attitude measurement system are used to observe transition of PAMS to steady state. The attitude measurement system is also used during later part of the mission to track steady-state cone angle and roll-angle performance. The attitude measurement system is based on an imaging technique. PAMS is equipped with an array of corner-cube retroreflectors, which are illuminated with a laser projected from the Shuttle. The reflected image from these retroreflectors is captured on a Shuttle charge-coupled device (CCD). Postmission analysis extracts the cone and roll angle of PAMS from these images.

Pams Simulation Results

To mimic the GAMES performance, it is desirable that PAMS be as similar as possible in design and in the environment it flies in. The high inclination of the GAMES subsatellite orbit cannot be realized on any shuttle missions. Nominal Shuttle orbit inclinations are less than 40 deg. Moreover, the Hitchhiker GAS canister assembly imposes design constraints on PAMS. The following is one of several suggested PAMS designs:

$$r_i = 5.91 \text{ cm}$$

$$t_f = 5.99 \text{ cm}, \qquad l_f = 13.6 \text{ cm}$$

$$t_b = 0.2 \text{ mm}, \qquad l_b = 31.4 \text{ cm}$$

$$\varrho_f = 2710 \text{ kg/m}^3 \quad \text{(aluminum)}$$

$$\varrho_b = 2710 \text{ kg/m}^3 \quad \text{(aluminum)}$$

Nominal simulation of PAMS attitude behavior also assumes mean values for the flux, geomagnetic index, accommodation coefficients, and global winds. The initial orbit is at an altitude of 160 nm at 28.5-deg inclination. The initial attitude of PAMS is −90 deg in pitch with respect to LVLH (to ensure an initial unstable mode) with maximum anticipated initial rate errors of 0.05, 0.1, and 0.1 deg/s in the body X, Y, and Z axes, respectively. Three magnetic torque rods, each 1/75 the strength of a TRANSIT 1B rod, are used for damping. These rods are aligned along the body axes. The chosen strength ensures damping within one day, a requirement imposed to accommodate certain Shuttle timeline constraints.

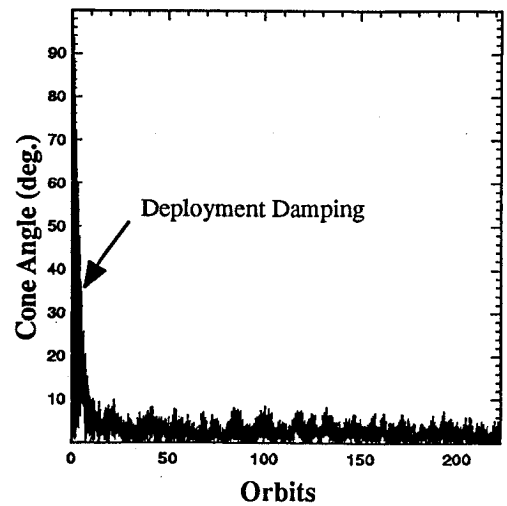

Fig. 8 Nominal PAMS simulation result.

Figure 8 depicts the cone angle time history of a nominal PAMS simulation. The peak steady-state cone angle over the 2-week mission is less than 9 deg. In general, the lower the orbital inclination and the lower the orbital altitude, the more stable the satellite attitude behavior, because of the less adverse effects of rotating atmosphere and global winds. Thus, the PAMS simulation, which is at a low Shuttle inclination orbit, shows smaller peak cone angle than the GAMES simulation, performed for an orbit inclination of 87 deg.

Once, the final design of PAMS is completed, Monte Carlo simulations need to be performed for several initial conditions and for different accommodation coefficients, flux, and geomagnetic indices. The PAMS actual attitude performance should lie within the envelope of cone-angle performance predicted by these Monte Carlo simulations. Moreover, errors in surface geometry and inertia due to manufacturing tolerances and its effect on performance needs to be addressed. The effect of Shuttle plume environment on PAMS attitude must also be considered.

Conclusions

Passive aerodynamically stabilized satellites do not require any power, active control systems, or long booms as gravity-gradient-stabilized satellites do. However, pure passive aerostabilization of satellites and utilization of miniature hysteresis damping rods has not yet been flight-demonstrated. This paper details the theory and procedure behind a high-fidelity simulator developed to predict post-deployment damping and aerostability. Simulation results of the experimental PAMS Shuttle test unit and the follow-on GAMES subsatellite indicate that passive aerostabilization is feasible.

Acknowledgment

This work was completed under Contract NAS1-18935 with Space Systems and Concepts Division at NASA Langley Research Center, Technical Monitor, J. W. Johnson.

References

[1]Pacini, L., and Skillman, D., "A Passive Aerodynamically Stabilized Satellite for Low Earth Orbit," AAS/AIAA Space Flight Mechanics Conference, Albuquerque, NM, AAS Paper 95-173, Feb. 1995.

[2]Ruck, G. T., Barrick, D. E., Stewart, W. D., and Krishbaum, C. K., *Radar Cross Section Handbook*, Plenum, New York, 1970, pp. 588–596.

[3]Hughes, P. C., *Spacecraft Attitude Dynamics*, Wiley, New York, 1986, pp. 248–264.

[4]Kaplan, M. H., Cwynar, D. J., and Alexander, S. G., "Anticipated Attitude Motion of Skylab for a 1979 Revisit Mission," *Journal of Spacecraft and Rockets*, Vol. 15, No. 4, 1978, pp. 219–223.

[5]Kaplan, M. H., Cwynar, D. J., and Alexander, S. G., "Simulation of Skylab Orbit Decay and Attitude Dynamics," 10th Space Simulation Conference, Bethesda, MD, 1978, pp. 123–130 (AIAA TP A79-10576 01-14).

[6]Alexander, S. G., and Glutch, B. K., "Prediction of Skylab Attitude Motion for Space Shuttle Revisit," NASA CR 152737, April 1977.

[7]Tate, V., "Investigation of Environmental Perturbations on a Passive Asymmetric Satellite," Dept. of Aerospace Engineering, Pennsylvania State Univ., Astronautics Research Rept. 76-1, University Park, PA, April 1976.

[8]Jacchia, L. G., "New Static Models of the Thermosphere and Exosphere with Emperical Temperature Profiles," Smithsonian Astrophysical Observatory, Special Rept. 313, 1970.

[9]Shatten, K. H., and Pesnell, W. D., "An Early Solar Dynamo Prediction: Cycle 23 ~ Cycle 22," *Geophysical Research Letters*, Vol. 20, No. 20, 1993, pp. 2275–2278.

[10]Hedin, A. E., et al., "Revised Global Model of Thermosphere Winds Using Satellite and Ground Based Observation," *Journal of Geophysics Research*, Vol. 96, 1991, pp. 7657–7688.

[11]Fischell, R. E., "Magnetic Damping of the Angular Motions of Earth Satellites," *ARS Journal*, Sept. 1961, pp. 1210–1217.

[12]Wertz, J. R., *Spacecraft Attitude Determination and Control*, D. Reidel, Dordrecht, The Netherlands, 1980, pp. 779–786.

[13]Flatley, T. W., and Henretty, D. A., "A Magnetic Hysteresis Model," Paper 38, *Proceedings of the Flight Mechanics/Estimation Theory Symposium* (Greenbelt, MD), May 1995.

[14]Kumar, R. R., Mazanek, D. D., and Heck, M. L., "Parametric and Classical Resonance in Passive Satellite Aero-Stabilization," AAS/AIAA Space Flight Mechanics Conference, Albuquerque, NM, AAS Paper 95-175, Feb. 1995.

[15]Bolotin, V. V., *The Dynamic Stability of Elastic Systems*, Holden–Day, San Francisco, 1964.

A. L. Vampola
Associate Editor